An analysis on tribological performance of CrCN coatings with different carbon contents in seawater (postprint)

Authors: Ye, YW, Wang, YX, Wang, CT, Li, JL, Yao, YR

Date: 2017-04-06T00:00:00+00:00

Abstract

CrCN coatings were deposited using the multi-arc ion plating with different C2H2 flow rates. Microstructures, mechanical and tribological performances were systematically investigated. The results showed that the peak intensity correlated to Cr7C3 crystal

Full Text

Preamble

Tribological Performance of CrCN Coatings with Different Carbon Contents in Seawater

Yuwei Ye, Yongxin Wang*, Chunting Wang, Jinlong Li, Yirong Yao
Key Laboratory of Marine Materials and Related Technologies, Zhejiang Key Laboratory of Marine Materials and Protective Technologies, Ningbo Institute of Materials Technology and Engineering, Chinese Academy of Sciences, Ningbo 315201, PR China

CrCN coatings were deposited via multi-arc ion plating at varying C_2H_2 flow rates, and their microstructures, mechanical properties, and tribological performances were systematically investigated. The results demonstrated that the peak intensity corresponding to the Cr_7C_3 crystal phase strengthened as the flow rate increased from 0 to 15 sccm, whereas it decreased when the C_2H_2 flow rate was further raised to 30 sccm. The hardness increased to 32.5 GPa at 10 sccm due to the formation of Cr_7C_3 phase and amorphous CN . CrCN coatings deposited at 10–15 sccm exhibited superior comprehensive performance, indicating their potential as protective coatings for tribological components in seawater applications.

Article History:
Received 25 April 2015
Received in revised form 19 June 2015
Accepted 2 July 2015
Available online 10 July 2015

Keywords: CrCN coating; C_2H_2 flow rate; Tribological performance; Seawater

Introduction

With the "blue revolution" of ocean exploitation emerging worldwide, increasing attention has focused on material performance in marine environments and the development of new materials suitable for such conditions. Mechanical components such as piston pumps, seal rings, and sliding or thrust bearings operating in water or seawater frequently experience severe damage during running-in periods, start/stop cycles, overloading, and overspeeding, imposing increasingly stringent requirements on protective and lubricating surface layers. CrN coatings have demonstrated promise as protective candidates for aqueous hydraulic systems due to their high hardness, good wear resistance, and corrosion resistance. However, CrN coatings sometimes fail to meet application demands, particularly under extreme conditions, because of their high friction coefficient.

Consequently, research on CrN coatings that retain their inherent advantages while achieving lower friction coefficients has become an academic focus in the self-lubricating coating field. Carbon, as a solid self-lubricating material, can significantly reduce the friction coefficient of hard coatings. Moreover, carbon addition to chromium nitride substantially affects coating microstructure and mechanical properties. Almer et al. found that carbon content in CrCN structures was closely related to coating stress, hardness, and critical load. Choi et al. reported that CrCN coatings with 20 at% C exhibited higher hardness and residual stress than CrN coatings. Cekada et al. indicated that adhesion between substrate and CrCN coating was lower than for CrN and CrC coatings. Furthermore, the friction coefficient and wear rate of CrCN coatings depend significantly on their carbon content. Tong et al. noted that CrCN coatings with 1.5 at% C showed the lowest friction coefficient when carbon content was below 5 at%. When carbon content reached 27 at%, both friction coefficients and wear rates decreased. These excellent tribological properties suggest CrCN coatings' potential as protective coatings in water hydraulic systems.

However, few investigations have examined the tribological behavior of CrCN coatings with varying carbon contents in seawater. To address this gap, CrCN coatings with different carbon contents were deposited on 316L stainless steel and silicon (100) wafers using multi-arc ion plating by adjusting the C_2H_2 flow rate. The composition, microstructure, mechanical properties, and tribological performance of these CrCN coatings in seawater were systematically investigated to elucidate how microstructure influences friction and wear properties in marine environments.

2.1. Deposition

Corresponding author. Tel.: +86 574 86685175; fax: +86 574 86685159.
E-mail address: yxwang@nimte.ac.cn (Y. Wang).

CrCN coatings were deposited on both Si (100) wafers and 316L stainless steel substrates (24 mm × 12 mm × 2 mm) using multi-arc ion plating. Prior to deposition, all substrates were ultrasonically cleaned in deionized water for 15 minutes and in ethanol for 20 minutes. After loading onto the substrate holder, the deposition chamber was evacuated to a background pressure below 4$×10^{-3}$ Pa. Substrates were then cleaned by Ar^+ bombardment for 2 minutes at negative bias voltages of -900 V, -1100 V, and -1200 V to remove oxide layers and surface contaminants. A pure Cr adhesive layer was first deposited for 30 minutes, followed by CrCN coating deposition.

During deposition, the working pressure was maintained at 0.3 Pa with the substrate holder rotating at 3 rpm. The CrCN coatings were prepared using a chromium target (purity $ 99.5*wt*_{2}$ (purity 99.99%) and C_2H_2 (purity 99.99%) atmosphere. Carbon concentration was controlled by adjusting the C_2H_2 flow rate while keeping the bias voltage at -70 V, current at 65 A, deposition temperature at 350°C, and deposition time at 120 minutes. The N_2 flow rate was fixed at 400 sccm, while C_2H_2 flow rates were varied from 0 to 30 sccm (0, 5, 10, 15, 20, 30 sccm). The pure CrN coating (0 sccm) and CrCN coatings deposited at 5, 10, 15, 20, and 30 sccm are hereafter designated as C2H2-0, C2H2-5, C2H2-10, C2H2-15, C2H2-20, and C2H2-30, respectively.

2.2. Characterization

Surface and cross-sectional images were examined using a field emission scanning electron microscope (FE-SEM, FEI Quanta FEG 250) equipped with EDS (OXFORD X-Max). Crystal phases were analyzed by X-ray diffraction (Bruker D8) using Cu Kα radiation (λ=0.154 nm) at 40 kV and 40 mA with a grazing incidence angle of 2°. The scanning range was 20° to 90° at 4°/min with a 0.02° step size.

XPS spectra were acquired using an X-ray photoelectron spectrometer (AXIS Ultra DLD) with an Al(mono) Kα source operated at 12 kV and 10 mA. Raman spectra of transfer layers were obtained with a Raman spectrometer (HR800) using a 532 nm Ar^+ laser with 1 cm^{-1} resolution. Typical acquisition time was 60 seconds, with spectra recorded from 1000–1800 cm^{-1} for reliable fitting.

Adhesion strength was evaluated using a scratch tester (CSM Revetest) with a conical diamond tip (0.2 mm radius, 120° taper angle) at a table speed of 5 mm/min, loading rate of 118 N/min, load range of 0–100 N, and scratch length of 5 mm under ambient conditions. LC1 corresponded to the first coating crack detected by acoustic emission, while LC2 indicated removal of >50% of the coating from the substrate. Scratch track damage was examined by JSM-5600 SEM.

Nanoindentation was performed on an MTS Nanoindenter G200 system with a Berkovich indenter using continuous stiffness measurement (CSM) mode. Hardness and elastic modulus were determined from load-displacement curves using the Oliver–Pharr method. The maximum indentation depth was 1000 nm, with six indentations performed on different areas of each sample for statistical reliability.

Corrosion behavior was assessed by polarization tests (EG&G 273) in artificial seawater prepared according to ASTM D1141-98 (composition listed in Table 1). The contact area was 1 cm^2, tests were conducted at ambient temperature (16$±$5°C), and the electrode potential was swept from -1.5 to 1.0 V at 1 mV/s.

2.3. Tribological Testing

Wear tests were conducted using a ball-on-disk configuration with WC balls (94% WC + 6% Co, 3 mm diameter) sliding against coated disks at room temperature (22$±2°C)*and*62±5×$S), where F is the normal load and S is the sliding distance.

3.1. Composition, Bonding Structure, and Morphology

Table 2 presents the chemical composition of CrCN coatings deposited at various C_2H_2 flow rates. Carbon content increased significantly from 0% to 21.32 at% with increasing C_2H_2 flow, while chromium and nitrogen contents decreased from 46.51% to 33.17% and 53.25% to 28.07%, respectively, confirming the strong influence of C_2H_2 flow rate on coating composition.

Surface roughness and thickness values are also listed in Table 2. Generally, surface roughness decreases with increasing carbon content, though macro-particles and pinholes that form during deposition can affect this trend. Coating thickness decreased from 3.98 to 3.02 m as C_2H_2 flow rates increased from 0 to 15 sccm, remaining relatively constant at higher flow rates.

Cross-sectional FE-SEM micrographs in Fig. 1 reveal the coating microstructures. A typical columnar structure is observed in the CrN coating (Fig. 1a), while a dense, compact structure emerges at 30 sccm C_2H_2 flow. This structural evolution is directly related to phase transformations within the coatings.

XRD spectra of CrCN coatings deposited at different C_2H_2 flow rates are shown in Fig. 2. Diffraction peaks corresponding to CrN(111), CrN(200), Cr_7C_3(151), CrN(220), Cr_2N(113), and Cr_2N(302) are evident. As C_2H_2 flow rate increases, CrN(111) and CrN(200) preferred orientations weaken and broaden, whereas Cr_7C_3(151) and CrN(220) intensities strengthen at lower flow rates before stabilizing at higher values. This behavior arises from structural differences between elemental carbon, chromium carbide, and chromium nitride. Carbon atoms can substitute for nitrogen in the chromium nitride lattice, disrupting the normal crystal arrangement and promoting transformation from crystalline to amorphous states.

To further analyze bonding structure changes, XPS spectra of C1s, Cr2p, and N1s were examined. Since no significant differences were observed among all CrCN coatings, only the deconvolved spectra for the 15 sccm sample are presented in Fig. 3. The Cr2p spectrum (Fig. 3a) fits to binding energies of 574.2 eV (Cr_7C_3), 575.7 eV (CrN), 576.3 eV (Cr_2N), 583.6 eV (Cr_7C_3), 585.4 eV (Cr_2O_3), and 586.4 eV (Cr_2O_3). The C1s peak (Fig. 3b) comprises four components centered at 282.8 eV (C-Cr), 284.6 eV (sp^2C-C), 286 eV (sp^3C-C), and 288.1 eV (C=O). The N1s core-level spectrum (Fig. 3c) deconvolves into three peaks at 397.8 eV (Cr-N), 399.3 eV (N-C), and 400.5 eV (N C), confirming amorphous CN formation after carbon incorporation. These results indicate the coexistence of CrN, Cr_2N, Cr_7C_3, and Cr_2O_3 phases, consistent with XRD analysis.

The calculated volume fractions of each carbon bond type are listed in Table 3. Hardness generally correlates with sp^3 fraction (higher sp^3 yields higher hardness), while friction coefficient relates to sp^2 fraction (higher sp^2 yields lower friction). Therefore, the C2H2-10 coating likely possesses the highest hardness and lowest friction coefficient among all samples.

High-resolution TEM results are presented in Fig. 4. The CrN coating (0 sccm) shows discrete (111), (200), (220), and (113) diffraction spots in the selected-area electron diffraction (SAED) pattern, confirming a cubic CrN phase and trigonal Cr_2N phase (Fig. 4a). At 10 sccm C_2H_2 flow (Fig. 4b), discrete (151) diffraction spots appear, and the coating exhibits a mixed nanocrystalline/amorphous microstructure. Similar nanocomposite structures are observed in Figs. 4c and 4d. Fig. 4c also reveals twinning structures consisting of CrN(200) planes, which hinder dislocation movement and improve coating toughness. Grain size decreases with increasing C_2H_2 flow rates from 0 to 10 sccm, then increases at higher flow rates—a key factor influencing coating performance.

3.2. Mechanical Properties

Critical loads (LC1 and LC2) for CrCN coatings are shown in Fig. 5. LC1, representing the first crack detected by acoustic emission, increases to 36 N at 15 sccm before decreasing to 28 N at 30 sccm. This initial cracking often originates from broken Cr micro-particles, which are softer and more fracture-prone than CrN or Cr_7C_3, or from crack propagation induced by the scratch stylus extruding pinholes. LC2, indicating cohesive failure (>50% coating removal), peaks at 86 N for the 10 sccm sample before declining to 63 N at 30 sccm. This trend reflects carbon-induced structural refinement, increased compressive stress, and reduced critical load at higher carbon contents. Scratch adhesion results are also influenced by substrate and coating hardness, surface roughness, friction coefficient between coating and stylus, substrate elastic properties, and coating thickness. With substrate properties and stylus type constant, and roughness/thickness values known from Table 2, the primary variables are coating hardness and friction coefficient.

Hardness, elastic modulus, H/E, and H^3/E^2 ratios are presented in Fig. 6. Hardness, H/E, and H^3/E^2 exhibit similar trends with C_2H_2 flow rate: hardness increases to 32 GPa at 10 sccm before decreasing to 22 GPa at 30 sccm, while elastic modulus, H/E, and H^3/E^2 all reach maximum values at 10 sccm. The enhanced hardness of CrCN over CrN coatings stems from high Cr–C and sp^3 bond contents. Wang reported that coating hardness correlates closely with sp^3 fraction, while Tong attributed hardness increases to solid solution hardening by carbon atoms. Additionally, Lim and Jung demonstrated that hardness increases with decreasing grain size. Thus, the 10 sccm sample achieves peak hardness through optimal carbon incorporation and grain refinement. The H/E and H^3/E^2 ratios correlate with coating durability and resistance to plastic deformation, providing reliable indicators of wear resistance. The C2H2-10 coating exhibits the highest H/E and H^3/E^2 values, indicating excellent mechanical and tribological properties.

3.3. Corrosion Properties

Polarization curves in artificial seawater are shown in Fig. 7, with corrosion current densities (i_{corr}) summarized in Table 4. The CrN coating exhibits low i_{corr}, which decreases with increasing C_2H_2 flow rate until reaching a minimum of ~7.27$×10^{-7}$ A/cm^2 at 10–15 sccm. This improvement is attributed to reduced grain size, denser structure, and fewer defects, consistent with TEM, SEM, and roughness results. Qin and Aung demonstrated that corrosion rates increase with grain size because smaller grains provide more nucleation sites for passive films, yielding higher passive film coverage and lower current density. Dense structures effectively prevent seawater permeation, enhancing corrosion resistance, while defects accelerate corrosion. Although no distinct defects like pinholes were observed in as-deposited coatings, microcracks can grow under cyclic stress combined with water molecule erosion, causing delamination around weak points.

At flow rates beyond 15 sccm, corrosion current densities increase, reaching ~8.31$×10^{-7}$ A/cm^2 at 30 sccm. Passivation occurs when the polarization potential increases from -0.2 to 0.2 V, indicating formation of a protective passive layer that temporarily prevents substrate exposure. Overall, CrCN coatings demonstrate good corrosion resistance.

3.4. Tribological Properties

Friction behaviors of CrCN coatings sliding against WC balls in artificial seawater are shown in Fig. 8a. The CrN coating exhibits rapid initial friction increase followed by a relatively steady-state after ~300 seconds. In contrast, CrCN coatings show a rapid initial increase, a noticeable friction decrease after ~150 seconds, and then transition to steady-state wear. The post-run-in decrease is attributed to counterface smoothing, hydrodynamic lubrication from continuous water presence, and deposition of Mg^{2+} and Ca^{2+} as $Mg(OH)_2$ and

$CaCO_3$ lubricating films.

Average friction coefficients and wear rates are presented in Fig. 8b. The CrN coating (0 sccm) shows the highest friction coefficient (~0.31) due to: (1) softer Cr phase flaking during sliding, (2) loose columnar structure forming through-film channels that accelerate crack initiation and propagation, and (3) absence of self-lubricating amorphous carbon. With increasing C_2H_2 flow rate, friction coefficients initially decrease, reaching a minimum at 10 sccm, then increase—closely related to surface roughness. Higher roughness reduces real contact area, concentrating load on fewer contact points and increasing friction.

Wear rates of CrCN coatings in seawater are lower than CrN, attributed to sp^2-hybridized carbon forming graphitic interface layers that reduce frictional shear resistance. Wear rates decrease to a minimum of ~7.686$×10^{-7}$ $mm^3/N \cdot m$ at 10 sccm due to high sp^2 content and good toughness, then increase to ~1.9519$×10^{-6}$ $mm^3/N \cdot m$ at 30 sccm. Shan noted that water can either accelerate wear by promoting crack growth and micro-fracture or reduce wear through tribo-chemical formation of smooth lubricating layers. Seawater represents a typical tribo-corrosion environment where mechanical and chemical degradation processes synergistically aggravate wear. Wear rate also correlates with coating-substrate adhesion; poor adhesion facilitates chipping and spalling during sliding, increasing wear.

Cross-sectional wear track profiles (Fig. 9) show maximum depths of ~0.6 m for CrN (0 sccm), decreasing to ~0.3 m at 15 sccm, then increasing to ~1 m at 30 sccm. The increased wear depth at 30 sccm likely results from enhanced corrosion and tribo-corrosion reactions. The relatively high wear depth of CrN is attributed to its low hardness and columnar structure, which provides straight diffusion channels for corrosive media, weakening compound bonding and accelerating wear.

All coatings remained intact during sliding, indicating no direct contact between tribo-balls and substrates. Wear track morphologies (Fig. 10) reveal that micro-particles undergo sufficient deformation to form smoother interfaces, while seawater accelerates corrosion. Wear pits form from micro-particle spalling during repetitive sliding, with seawater corrosion exacerbating this process. Flake pits observed in Figs. 10c and 10d (20 and 30 sccm samples) result from crack propagation under cyclic sliding due to low hardness and poor adhesion. As plastic deformation accumulates, cracks preferentially form beneath the contact region under high compressive stress, extending with further deformation and causing delamination. In contrast, the 10 sccm coating shows no obvious pits, attributed to its high hardness and good corrosion resistance.

EDS analysis of wear tracks (Fig. 11) reveals Na, S, and Cl elements on both coating surfaces and within wear tracks, indicating transfer from artificial seawater. Stronger Na and Cl signals in wear tracks result from their ability to retain more seawater. Tungsten signals confirm material transfer from the WC counterpart. The presence of Cr, C, N, and O indicates oxidation occurred,

consistent with previous reports. Low friction is attributed to graphitization and tribolayer formation during cyclic sliding.

Raman spectra of WC ball contact surfaces (Fig. 12) show a peak at ~1580 cm^{-1}, confirming sp^2-hybridized carbon in the tribolayer. The planar 2D graphite-like structure reduces dangling σ bonds, minimizing adhesive interactions between WC ball and coating. At 0 sccm, no obvious graphite character is observed. The sp^2 peak intensity increases to a maximum at 10 sccm, consistent with sp^2 fraction content. Overall, CrCN tribological behavior is closely related to carbon content, with coatings deposited at 10–15 sccm C_2H_2 flow demonstrating optimal performance for seawater tribo-component applications.

4. Conclusions

CrCN coatings were deposited by multi-arc ion plating at various C_2H_2 flow rates to investigate carbon content effects on microstructure, mechanical properties, and tribological performance in seawater. The main conclusions are:

1. Carbon concentration increased gradually from 0 to 21.32 at% with C_2H_2 flow rate, existing primarily as Cr–C, sp^2, and sp^3 bonds.
2. Friction coefficients varied significantly with C_2H_2 flow rate in seawater, reaching a minimum at 10 sccm and maximum at 0 sccm. This correlates with sp^2 bond fraction and columnar structure—graphitic sp^2 carbon reduces friction, while columnar structures promote micro-fracture during sliding.
3. The lowest wear rate occurred at 10 sccm, coinciding with the shallowest wear track depth, resulting from high hardness, excellent toughness, and superior corrosion resistance.

Acknowledgments

This work was supported by the National Natural Science Foundation of China (51161008 and 51202261) and the National Basic Research Program of China (973 Program) (Grant No. 2013CB632300). The authors gratefully acknowledge this financial support.

References

[1] Chen BB, Wang JZ, Yan FY. Friction and wear behaviors of several polymers sliding against GCr15 and 316 steel under the lubrication of sea water. Tribol Lett 2011;42:17–25.
[2] Ye YW, Wang YX, Chen H, Li JL, Zhou SG, Xue QJ. Influences of bias voltage on the microstructures and tribological performances of Cr–C–N coatings in seawater. Surf Coat Technol 2015;270:305–13.
[3] Shan L, Wang Y, Li J, Li H, Wu X, Chen J. Tribological property of TiN, TiCN and CrN coatings in seawater. China Surf Eng 2013;26(6):86–92.

[4] Yao SH, Su YL. The tribological potential of CrN and Cr(C,N) deposited by multi-arc PVD process. Wear 1997;212:85–94.
[5] Wang QZ, Zhou F, Wang XN, Chen KM, Wang ML, Qian T, et al. Comparison of tribological properties of CrN, TiCN and TiAlN coatings sliding against SiC balls in water. Appl Surf Sci 2011;257:7813–20.
[6] Navinsek B, Panjan P. Oxidation resistance of PVD Cr, Cr–N and Cr–N–O hard coatings. Surf Coat Technol 1993;59:244–8.
[7] Ichimura H, Kawana A. High temperature oxidation of ion-plated CrN films. J Mater Res 1994;9:151–5.
[8] Liu C, Bi Q, Matthews A. EIS comparison on corrosion performance of PVD TiN and CrN coated mild steel in 0.5 N NaCl aqueous solution. Corros Sci 2001;43:1953–61.
[9] Bertrand G, Mahdjoub H, Meunier C. A study of the corrosion behaviour and protective quality of sputtered chromium nitride coatings. Surf Coat Technol 2000;126:199–209.
[10] Wang J, Zhang A, Wang L. The influence of metal alloyed on the structure and wear properties of CrN coatings. Lubr Eng 2008;33:30–2.
[11] Knotek O, Loefer F, Kreme G. Multicomponent and multilayer PVD coatings for cutting tools. Surf Coat Technol 1992;54:241–8.
[12] Huang JX, Wan SH, Wang LP, Xue QJ. Tribological properties of Si-doped graphite-like amorphous carbon film of PEEK rubbing with different counterparts in SBF medium. Tribol Lett 2015;57:10–7.
[13] Guan XY, Wang LP. The tribological performances of multilayer graphite-like carbon (GLC) coatings sliding against polymers for mechanical seals in water environments. Tribol Lett 2012;47:67–78.
[14] Guan XY, Lu ZB, Wang LP. Achieving high tribological performance of graphite-like carbon coatings on Ti6Al4V in aqueous environments by gradient interface design. Tribol Lett 2011;44:315–25.
[15] Huang JX, Wang LP, Liu B, Wan SH, Xue QJ. In vitro evaluation of the tribological response of Mo-doped graphite-like carbon film in different biological media. ACS Appl Mater Interfaces 2015;7:2772–83.
[16] Almer J, Oden M, Hakansson G. Microstructure, stress and mechanical properties of arc-evaporated Cr–C–N coatings. Thin Solid Films 2001;385:190–7.
[17] Choi E, Kang M, Kwon D, Shin D, Kim D. Comparative studies on microstructure and mechanical properties of CrN, Cr–C–N and Cr–Mo–N coatings. J Mater Process Technol 2007;187–188:566–70.
[18] Cekada M, Macek M, Merl DK, Panjan P. Properties of Cr(C,N) hard coatings deposited in Ar-C_2H_2-N_2 plasma. Thin Solid Films 2003;433:174–9.
[19] Wu ZL, Lin J, Moore JJ, Lei MK. Microstructure, mechanical and tribological properties of Cr–C–N coatings deposited by pulsed closed field unbalanced magnetron sputtering. Surf Coat Technol 2009;204:931–5.
[20] Tong CY, Lee JW, Kuo CC, Huang SH, Chan YC, Chen HW, et al. Effects of carbon content on the microstructure and mechanical property of cathodic arc evaporation deposited CrCN thin films. Surf Coat Technol 2013;231:482–6.
[21] Hu PF, Jiang BL. Study on tribological property of CrCN coating based

on magnetron sputtering plating technique. Vacuum 2011;85:994–8.
[22] Oliver WC, Pharr GM. An improved technique for determining hardness and elastic modulus using load and displacement sensing indentation experiments. J Mater Res 1992;7:1564–83.
[23] Boxman RL, Goldsmith S. Macroparticle contamination in cathodic arc coatings: generation, transport and control. Surf Coat Technol 1992;52:39–50.
[24] Wang RY, Wang LL, Liu HD, Yan SJ, Chen YM, Fu DJ, et al. Synthesis and characterization of CrCN–DLC composite coatings by cathodic arc ion-plating. Nucl Instrum Methods Phys Res B 2013;307:185–8.
[25] Healy MD, Smith DC, Rubiano RR, Elliott NE, Springer RW. Use of tetra-neopentylchromium as a precursor for the organometallic chemical vapor deposition of chromium carbide: reinvestigation. Chem Mater 1994;6:448–53.
[26] Shi Y, Long S, Fang L, Yang S, Pan F. Effect of nitrogen content on the properties of CrNxOyCz coating prepared by DC reactive magnetron sputtering. Appl Surf Sci 2008;254:5861–7.
[27] Vyas A, Shen YG, Zhou ZF, Li KY. Nano-structured CrN/CNx multilayer films deposited by magnetron sputtering. Compos Sci Technol 2008;68:2922–9.
[28] Agostinelli E, Battistoni C, Fiorani D, Mattogno G, Nogues M. An XPS study of the electronic structure of the $ZnxCd_1$ xCr_2 (X = S, Se) spinel system. J Phys Chem Solids 1989;50:269–72.
[29] Tandon RK, Payling R, Chenhall BE, Crisp PE, Ellis J, Baker RS. Application of X-ray photoelectron spectroscopy to the analysis of stainless-steel welding aerosols. Appl Surf Sci 1985;20:527–37.
[30] Goretzki H, Rosenstiel PV, Mandziej S, Fres Z. Small area MXPS- and TEM-measurements on temper-embrittled 12% Cr steel. Anal Chem 1989;333:451–2.
[31] Dai W, Ke PL, Wang AY. Microstructure and property evolution of Cr-DLC films with different Cr content deposited by a hybrid beam technique. Vacuum 2011;85:792–7.
[32] Zhou F, Adachi K, Kato K. Friction and wear property of a-CNx coatings sliding against ceramic and steel balls in water. Diam Relat Mater 2005;14:1711–20.
[33] Bismarck A, Tahhan R, Springer J, Schulz A, Klapotke TM, Zell H. Influence of fluorination on the properties of carbon fibres. J Fluor Chem 1997;84:127–34.
[34] Matron D, Boya KJ, AI-Bayali AH, Todorov SS, Rabalais JW. Carbon nitride deposited using energetic species: a two-phase system. Phys Rev Lett 1994;73:118–21.
[35] Cheng YH, Qiao XL, Chen JG, Wu YP, Xie CS, Wang YQ, et al. Dependence of the composition and bonding structure of carbon nitride films deposited by direct current plasma assisted pulsed laser ablation on the deposition temperature. Diam Relat Mater 2002;11:1511–7.
[36] Lin Y, Munroe RR. Deformation behavior of complex carbon nitride and metal nitride based bi-layer coatings. Thin Solid Films 2009;517:4862–6.
[37] Ye YW, Wang YX, Chen H, Li JL, Yao YR, Wang CT. Doping carbon to improve the tribological performance of CrN coatings in seawater. Tribol Int

2015;90:362–71.
[38] Warcholinski B, Gilewicz A. Effect of substrate bias voltage on the properties of CrCN and CrN coatings deposited by cathodic arc evaporation. Vacuum 2013;90:145–50.
[39] Odén M, Almer J, Håkansson G. The effects of bias voltage and annealing on the microstructure and residual stress of arc-evaporated Cr–N coatings. Surf Coat Technol 1999;120–121:272–6.
[40] Wang QZ, Zhou F, Ding XD, Zhou ZF, Wang CD, Zhang WJ, et al. Microstructure and water-lubricated friction and wear properties of CrN(C) coatings with different carbon contents. Appl Surf Sci 2013;268:579–87.
[41] Lim Yee Y, Chaudhri, Munawar M. The influence of grain size on the indentation hardness of high-purity copper and aluminium. Philos Mag A 2002;82:2071–80.
[42] Jung BB, Lee HK, Park HC. Effect of grain size on the indentation hardness for polycrystalline materials by the modified strain gradient theory. Int J Solids Struct 2013;50:2719–24.
[43] Sakharova NA, Fernandes JV, Oliveira MC, Antunes JM. Influence of ductile interlayers on mechanical behaviour of hard coatings under depth-sensing indentation: a numerical study on TiAlN. J Mater Sci 2010;45:3812–23.
[44] Qin LY, Lian JS, Jiang Q. Effect of grain size on corrosion behavior of electrodeposited bulk nanocrystalline Ni. Trans Nonferr Met Soc China 2010;20:82–9.
[45] Aung NN, Zhou W. Effect of grain size and twins on corrosion behaviour of AZ31B magnesium alloy. Corros Sci 2010;52:589–94.
[46] Shan L, Wang Y, Li J, Li H, Wu X, Chen J. Tribological behaviours of PVD TiN and TiCN coatings in artificial seawater. Surf Coat Technol 2013;226:40–50.
[47] Roos J, Celis JP, Vancoille E, Veltrop H, Boelens S, Jungblut F, et al. Inter-relationship between processing, coating properties and functional properties of steered arc physically vapour deposited (Ti,Al)N and (Ti,Nb)N coatings. Thin Solid Films 1990;193:547–56.
[48] Neville A, Morina A, Haque T, Voong M. Compatibility between tribological surfaces and lubricant additives—how friction and wear reduction can be controlled by surface/lube synergies. Tribol Int 2007;40:1680–95.
[49] Wang J, Yan Y, Xue Q. Tribological behavior of PTFE sliding against steel in sea water. Wear 2009;267:1634–41.
[50] Field SK, Jarratt M, Teer DG. Tribological properties of graphite-like and diamond-like carbon coatings. Tribol Int 2004;37:949–56.
[51] Shan L, Wang Y, Li J, Chen J. Effect of N_2 flow rate on microstructure and mechanical properties of PVD CrNx coatings for tribological application in seawater. Surf Coat Technol 2014;242:74–82.
[52] Al-Samarai Riyadh A, Haftirman, Ahmad Khiarel Rafezi, Al-Douri Y. The influence of roughness on the wear and friction coefficient under dry and lubricated sliding. Int J Sci Eng Res 2012;3:1–6.
[53] Landolt D, Mischler S, Stemp M. Electrochemical methods in tribocorrosion: a critical appraisal. Electrochim Acta 2001;46:3913–29.

[54] Liu C, Leyland A, Bi Q, Matthews A. Corrosion resistance of multi-layered plasma-assisted physical vapour deposition TiN and CrN coatings. Surf Coat Technol 2001;141:164–73.
[55] Wang J, Chen J, Chen B, Yan F, Xue Q. Wear behaviors and wear mechanisms of several alloys under simulated deep-sea environment covering seawater hydrostatic pressure. Tribol Int 2012;56:38–46.
[56] Wang YX, Wang LP, Zhang GA, Wang SC, Wood RJK, Xue QJ. Effect of bias voltage on microstructure and properties of Ti-doped graphite-like carbon films synthesized by magnetron sputtering. Surf Coat Technol 2010;205:793–800.

Figures

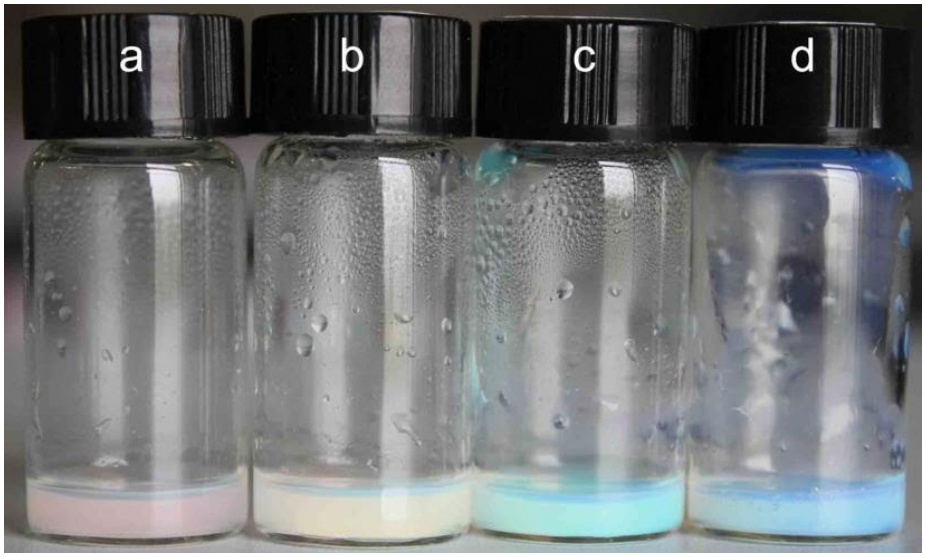

Figure 1: Figure 3